

Article

Immobilization of TiO₂ Nanoparticles in Hydrogels Based on Poly(methyl acrylate) and Succinamide Acid for the Photodegradation of Organic Dyes

Xiaomeng You [†], Hailong Huang [†], Ran Zhang, Zhongli Yang, Min Xu ^{*†} , Xuelu Wang ^{*} and Yefeng Yao ^{*}

Physics Department & Shanghai Key Laboratory of Magnetic Resonance, School of Physics and Electronic Science, East China Normal University, North Zhongshan Road 3663, Shanghai 200062, China; yxmmusian@outlook.com (X.Y.); huanghailong@sinap.ac.cn (H.H.); zhangran@whu.edu.cn (R.Z.); ZhongliYang2021@outlook.com (Z.Y.)

* Correspondence: xumin@phy.ecnu.edu.cn (M.X.); xlwang@phy.ecnu.edu.cn (X.W.); yfyao@phy.ecnu.edu.cn (Y.Y.)

[†] These authors contributed equally.

Abstract: Hydrogels have excellent properties that make them ideally suited as host matrices for the immobilization of photoreactive materials such as TiO₂ nanoparticles that serve as catalysts in the photodegradation of organic dyes, which is of great importance in practical water pollution treatment applications. However, the application of hydrogels for this purpose remains poorly studied. The present study addresses this issue by developing two types of hydrogels based on poly(methyl acrylate) and succinamide acid with embedded TiO₂ nanoparticles for use as photocatalysts in the photodegradation of organic dyes. The results of the analysis demonstrate that the TiO₂ nanoparticles are distributed uniformly in the hydrogel matrices, and the hydrogels maintain their original structures after use. The photodegradation efficiencies of the developed TiO₂-hydrogels are demonstrated to be reasonably close to that of freely distributed TiO₂ nanoparticles in solution for four different organic dyes. In addition, the results of degradation-regeneration cycling tests demonstrate that immobilizing the TiO₂ nanoparticles into the hydrogels greatly reduces their loss during utilization, and the photocatalysts can be easily reused. In fact, the two TiO₂-hydrogels retain reasonably high photocatalytic degradation performance after four degradation-regeneration cycles.

Keywords: photocatalyst; hydrogel; photocatalytic reaction; degradation



Citation: You, X.; Huang, H.; Zhang, R.; Yang, Z.; Xu, M.; Wang, X.; Yao, Y. Immobilization of TiO₂ Nanoparticles in Hydrogels Based on Poly(methyl acrylate) and Succinamide Acid for the Photodegradation of Organic Dyes. *Catalysts* **2021**, *11*, 613. <https://doi.org/10.3390/catal11050613>

Academic Editors:
Dionissios Mantzavinos and
Danilo Russo

Received: 6 April 2021
Accepted: 8 May 2021
Published: 11 May 2021

Publisher's Note: MDPI stays neutral with regard to jurisdictional claims in published maps and institutional affiliations.



Copyright: © 2021 by the authors. Licensee MDPI, Basel, Switzerland. This article is an open access article distributed under the terms and conditions of the Creative Commons Attribution (CC BY) license (<https://creativecommons.org/licenses/by/4.0/>).

1. Introduction

Water is among the most essential substances for the existence of life on earth. Nevertheless, the wastewater discharged from factories and laboratories has caused serious water pollution in recent years [1–3]. In particular, textile, paper, plastic, and cosmetic industries discharge large amounts of organic dyes [4], which are toxic and can cause serious ecological problems. Therefore, the development of sustainable methods of eliminating organic dye pollutants from wastewater is essential for preserving quality of life. Among these presently available methods, photocatalytic degradation is particularly promising owing to its potential environmental friendliness, and it has been demonstrated to realize the efficient degradation of various organic pollutants in wastewater treatment applications [5–7]. In this regard, titanium dioxide (TiO₂) is one of the most widely used semiconductor photocatalysts in the field of photocatalytic water decomposition [8–10], as well as in environmental remediation applications due to its high photocatalytic activity, chemical stability, low cost, non-toxicity, and stability during reactions [11–14].

Typically, most photocatalysts employed in wastewater treatment applications exist in powder form and are directly mixed in wastewater to generate a solid-liquid suspension. Pollutant degradation is then conducted under light irradiation, and the photocatalyst powder must be subsequently separated from the solid-liquid mixture and retained for

later use. However, the subsequent separation of the solid-liquid mixture is rather difficult in practical wastewater treatment applications [15,16]. This is not the case when conducting photodegradation tests in the laboratory because the solution samples involved are very small, and the solid and liquid phases can be separated almost completely by centrifugation. Nonetheless, the complete separation of relatively low-density catalysts, such as graphitic carbon nitride ($g\text{-C}_3\text{N}_4$) and aerogel photocatalysts, is difficult to achieve even at high rotational speeds of 10,000 rpm. While this issue is commonly addressed by passing solid-liquid mixtures through disposable syringe filters, this results in catalyst loss, which is unacceptable for cyclic degradation-regeneration performance testing due to the detrimental effect on measurement accuracy caused by the progressively decreasing catalyst concentration. Moreover, this will increase the cost of experiments when working with expensive catalysts. This issue has been addressed in recent years by immobilizing powdered catalysts on support materials. For example, Li et al. [17] developed a novel double-cylindrical-shell (DCS) photoreactor with an immobilized monolayer of TiO_2 coated on silica gel beads, and the proposed photoreactors were successfully applied for the degradation of rhodamine B (RhB) and methyl orange (MO) organic dyes. Lei et al. [18] demonstrated that TiO_2 nanoparticles immobilized in a polyvinyl alcohol (PVA) matrix obtained excellent photocatalytic activity. In this regard, TiO_2 nanoparticles have been effectively immobilized in a wide variety of matrix materials such as glass, activated carbon, silica, carbon nanotubes, and polymers [16,19]. Recently, hydrogels have been employed as novel matrix materials for immobilizing TiO_2 nanoparticles [20–24]. Hydrogels represent particularly excellent candidates for use as matrix materials in the immobilization of TiO_2 nanoparticle photocatalysts for photodegradation applications. For example, hydrogels have three-dimensional (3D) cross-linked polymeric networks with volumetric and other properties that are responsive to pH and temperature [24], and readily adsorb organic pollutants [25]. Moreover, most hydrogels have good mechanical strength, thermal stability, and electrical conductivity, which make them useful in a wide range of fields such as water purification, biomimetic materials, and electrochemistry [25–27]. However, the use of hydrogels for photocatalyst immobilization in photocatalytic wastewater treatment applications remains poorly studied.

This issue is addressed in the present work by developing two types of hydrogels based on poly (methyl acrylate) (PMA) and succinamide acid (SAA) with embedded TiO_2 nanoparticles for use as photocatalysts in the photodegradation of four different organic dyes, including MO, methylene blue, RhB, and bright green. The photodegradation efficiencies of the developed TiO_2 -hydrogel materials, denoted herein as PMA- TiO_2 and SAA- TiO_2 , are demonstrated to be reasonably close to that of freely distributed TiO_2 nanoparticles in solution for all four organic dyes. Moreover, the immobilization of TiO_2 nanoparticles in the hydrogels eliminates the need to separate solid and liquid phases after conducting the photodegradation process, which enhances the recovery of the photocatalysts and promotes their easy reuse. In addition, the two TiO_2 -hydrogels retain high photocatalytic degradation performance for RhB after four degradation-regeneration cycles. As such, the proposed strategy of physically immobilizing TiO_2 nanoparticles in hydrogels may promote the development of photocatalytic devices suitable for practical large-scale applications.

2. Results and Discussion

2.1. Characterizations

The present work employed commercial P25 TiO_2 nanoparticles with phase concentrations of 76% anatase and 24% rutile by mass [28], which provides a greater photocatalytic activity than either anatase or rutile [29]. The crystalline structure of the P25 TiO_2 nanoparticles is verified by the XRD pattern shown in Figure 1, where characteristic peaks corresponding to the anatase phase appear at 25.5° , 38.0° , 48.2° , 54.5° , 62.9° , and 75.2° , and the characteristic peaks corresponding to the rutile phase are observed at 27.6° , 36.3° , 41.5° , 56.9° , and 64.3° . Accordingly, the TiO_2 nanoparticles are a mixed phase. The energy dis-

perse spectroscopy (EDS) elemental mapping images shown in Figure 2 of a representative PMA-TiO₂ hydrogel sample indicate that the elements Ti, O, and C are homogeneously distributed near the sample surface.

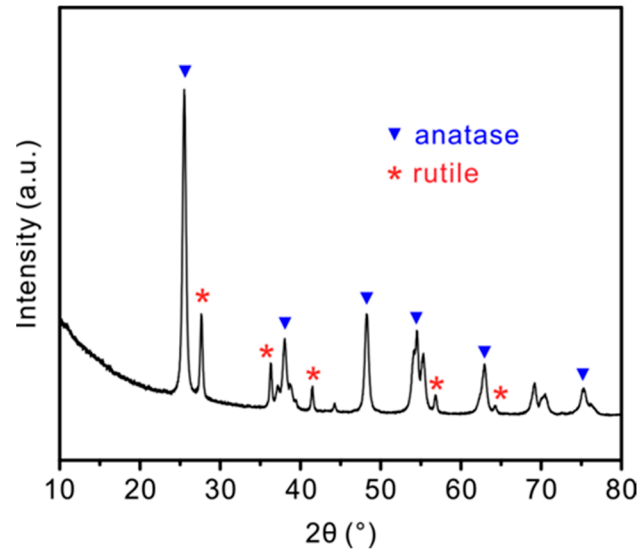


Figure 1. XRD pattern of the commercial P25 TiO₂ nanoparticles employed in the work.

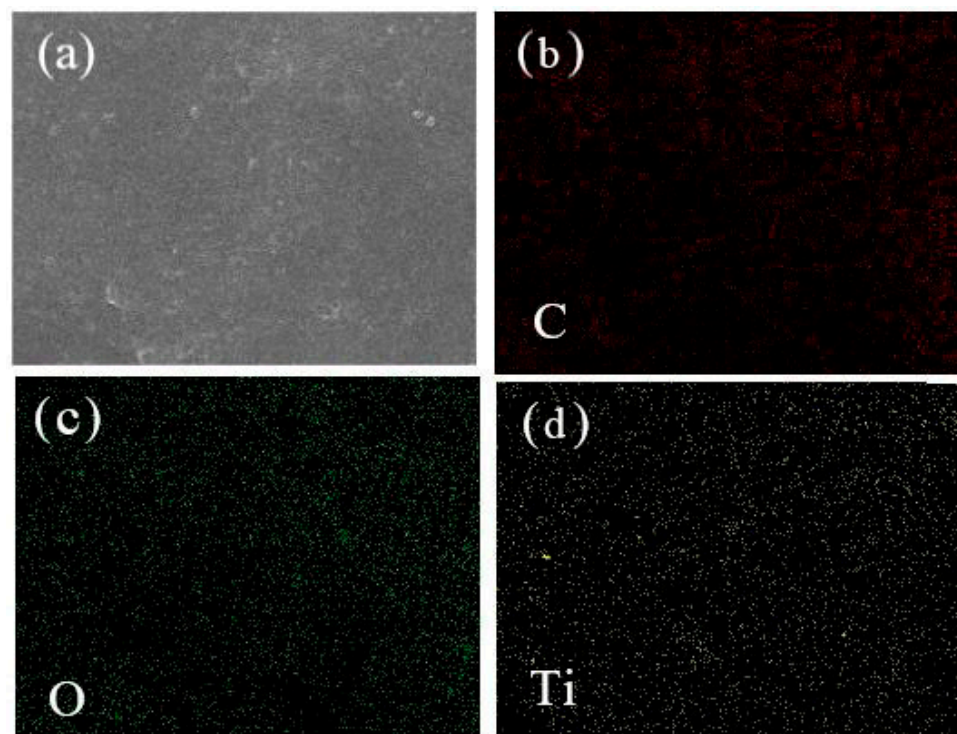


Figure 2. (a) SEM image of PMA- TiO₂ sample; (b) C, (c) O and (d) Ti EDS elemental mapping images of a representative PMA-TiO₂ hydrogel sample.

The synthesized TiO₂-hydrogel samples had diameters of 2 cm and thicknesses of about 0.5 cm after drying. The precursor solution employed for preparing PMA-TiO₂ samples had a density close to that of water. Therefore, the added 20.0 mg of TiO₂ nanoparticles fell to the bottom, leaving a thin layer of TiO₂ nanoparticles near the bottom surface. This is shown by the image given in Figure 3a. Meanwhile, the top surface of the PMA-TiO₂ samples remained transparent, as shown in Figure 3b. This conforms to what has been

observed previously [25]. The SAA hydrogel was light yellow in color, and was somewhat transparent, as shown in Figure 3c. In contrast to the PMA-TiO₂ samples, the 5.0 mg of TiO₂ nanoparticles added to the SAA precursor solution were uniformly dispersed within the hydrogel due to the high density and viscosity of the precursor solution, as shown in Figure 3d. Here, only 5.0 mg of TiO₂ nanoparticles was added to the SAA precursor solution because the added nanoparticles greatly reduced the transparency of the SAA hydrogel, and a larger concentration of nanoparticles would unacceptably diminish the availability of light in the subsequent photodegradation experiments.

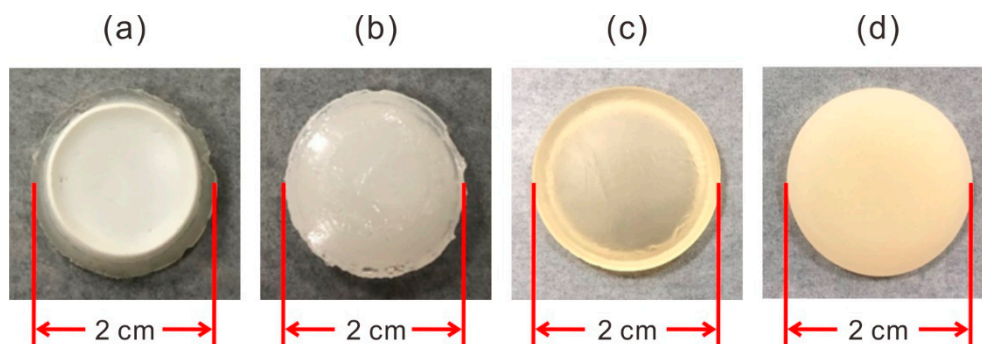


Figure 3. Images of standard hydrogel samples: (a) bottom side of a PMA-TiO₂ sample (20.0 mg added TiO₂) with a thin layer of TiO₂ nanoparticles near the surface; (b) top side of the PMA-TiO₂ sample with a transparent surface; (c) bottom side of an SAA hydrogel sample (5.0 mg added TiO₂) with a transparent surface; (d) top side the SAA-TiO₂ sample with a uniform distribution of TiO₂ nanoparticles.

2.2. Photocatalytic H₂ Production

The excellent adsorption capacity of the hydrogel can be expected to facilitate the photocatalytic reaction of the uniformly dispersed TiO₂ nanoparticles in the hydrogel due to a continuous adsorption of small molecules. This issue was investigated by evaluating the H₂ production performance obtained by different concentrations of freely dispersed TiO₂ nanoparticles in deionized water with 10 mL TEOA added as a sacrificial reagent under a 300 W xenon lamp as an ultraviolet-visible (UV-Vis) light source, and comparing those results with those obtained for PMA-TiO₂ samples with different TiO₂ nanoparticle loadings and the SAA-TiO₂ sample with 5 mg of added TiO₂ nanoparticles.

As shown in Figure 4, the H₂ production rates of freely dispersed TiO₂ nanoparticles were 1.65, 3.02, and 6.16 $\mu\text{mol/h}$ for TiO₂ concentrations of 5.0 mg, 10.0 mg, and 20.0 mg, respectively. We also note from the figures that the H₂ evolution obtained was basically linear with respect to the irradiation time for all three TiO₂ concentrations.

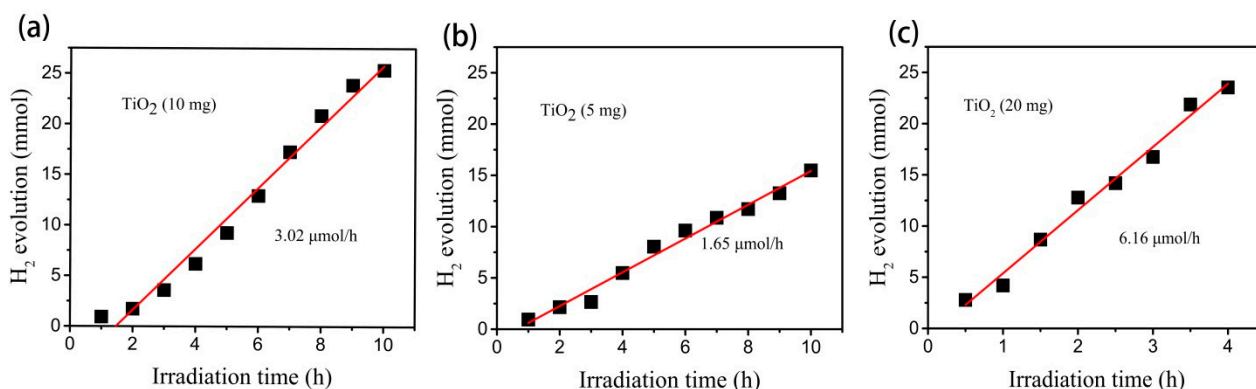


Figure 4. Photocatalytic H₂ evolution rates obtained with different concentrations of TiO₂ nanoparticle powder in deionized water with 10 mL triethanolamine (TEOA) added as the sacrificial reagent and a 300 W xenon lamp as a light source: (a) 5.0 mg; (b) 10.0 mg; (c) 20.0 mg.

For testing the H₂ evolution performance of the PMA-TiO₂ samples, the thin layer of TiO₂ nanoparticles on the bottom surface of the hydrogel sample was exposed to irradiation during the experiments. As shown in Figure 5, the H₂ production rates of the PMA-TiO₂ samples were 0.86 and 1.28 μmol/h for TiO₂ nanoparticle loadings of 10.0 mg and 20.0 mg, respectively. We note that the H₂ evolution rate increases with increasing photocatalyst content, even though the area of irradiation remains constant, which demonstrates the impact of the TiO₂ nanoparticle density at the surface of the PMA hydrogel on H₂ production.

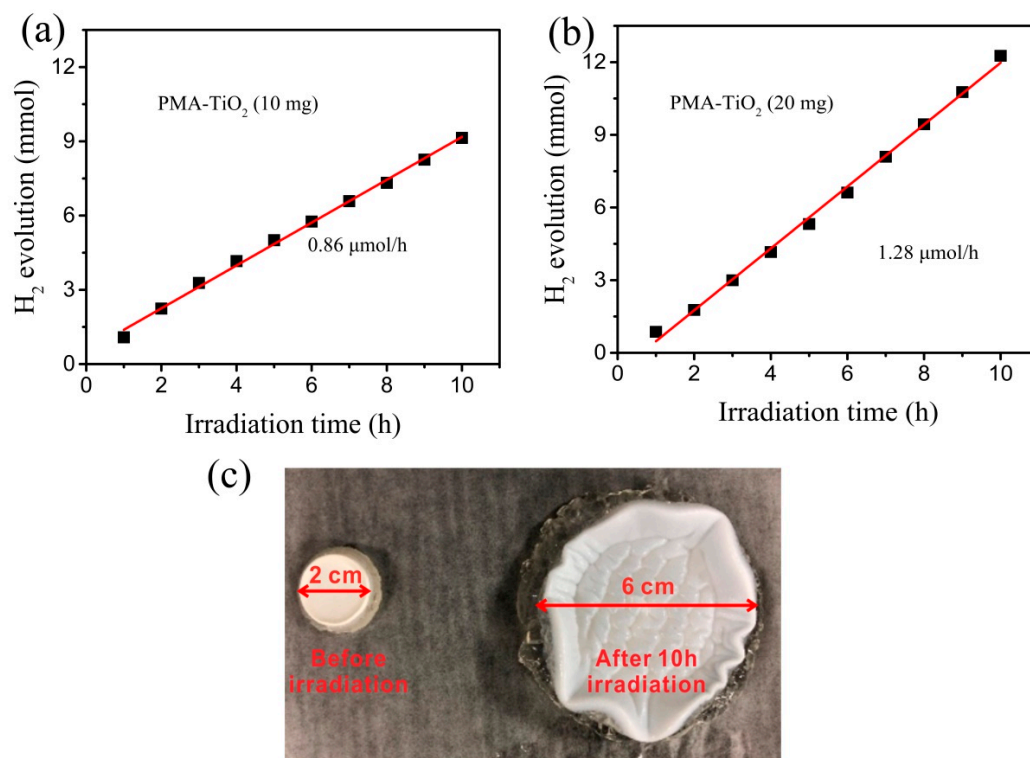


Figure 5. Photocatalytic H₂ evolution rates obtained with different concentrations of TiO₂ nanoparticles in the PMA hydrogel: (a) 10.0 mg; (b) 20.0 mg. (c) Images of a PMA-TiO₂ sample (20.0 mg TiO₂) before and after reaction process involving 10 h of irradiation.

The results also indicate that the photocatalytic efficiencies of the PMA-TiO₂ samples with 10.0 mg and 20.0 mg of TiO₂ nanoparticles were 28.5% and 20.8%, respectively, of the freely dispersed TiO₂ nanoparticles with equivalent photocatalyst concentrations. While the greater concentration of TiO₂ nanoparticles dispersed in the PMA hydrogel increased the hydrogen production of PMA-TiO₂, the efficiency of the photocatalyst in PMA-TiO₂ did not increase with increasing TiO₂ content to the same extent as the freely dispersed TiO₂ nanoparticles. This could potentially be attributable to the two-dimensional (2D) nature of the PMA-TiO₂ sample surface, which limits interactions between the photocatalyst and reactive components in the liquid phase relative to the 3D conditions of the freely dispersed TiO₂ nanoparticles in the solution. However, we note from Figure 5c that the PMA-TiO₂ sample absorbed a large volume of solution, and the diameter of the sample after 10 h of reaction was greater than its original diameter by a factor of about three. The high absorbance of the hydrogel facilitated 3D interactions between the solution and the embedded TiO₂ nanoparticles, and presumably enabled the generated hydrogen to also be desorbed quickly. Therefore, we conclude that the primary factor affecting the photocatalytic performance of the PMA-TiO₂ sample was that the immobilization of the TiO₂ particles in the hydrogel decreased the availability of incident light.

As shown Figure 6, the H₂ production rate of the SAA-TiO₂ sample with a 5.0 mg TiO₂ nanoparticle loading was 0.35 μmol/h, which represents a photocatalytic efficiency that is

21.2% that of the 5.0 mg of freely dispersed TiO_2 nanoparticles in the solution. This is similar to the relative photocatalytic efficiency of the PMA- TiO_2 sample with the 20.0 mg TiO_2 loading. We further note from Figure 6b that the SAA- TiO_2 sample also adsorbed a large amount of solution, and the diameter of the sample after 5 h of reaction was also greater than its original diameter by a factor of about 3. Moreover, we note that the transparency of the SAA- TiO_2 sample was significantly improved after absorbing the solution. The uniform milkiness of the sample also demonstrates that the TiO_2 nanoparticles are evenly dispersed in the SAA hydrogel, which is favorable for promoting the photocatalytic reaction.

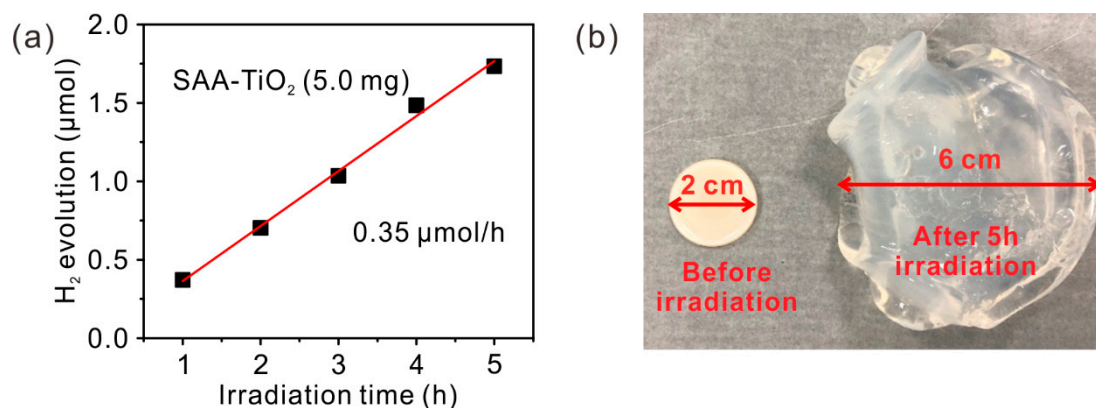


Figure 6. (a) Photocatalytic H_2 evolution rates obtained by an SAA- TiO_2 sample with 5.0 mg added TiO_2 . (b) Images of the SAA- TiO_2 sample before and after the reaction process involving 5 h of irradiation.

As discussed above with respect to H_2 generation, the excellent solution absorbance of the hydrogel samples enables contact between the TiO_2 nanoparticles and the surrounding solution even though the nanoparticles are immobilized through embedding. While this embedding does decrease the availability of light, and, with it, the photocatalytic efficiency, it also enables the easy removal of the active photocatalyst from solution, which can be expected to greatly improve the efficiency of wastewater treatment applications.

2.3. Photodegradation of Organic Dyes

The concentrations of MO, methylene blue, RhB, and bright green employed in the photodegradation experiments were all 20 mg/L. The photocatalysts considered were 20.0 mg and 5.0 mg of freely dispersed TiO_2 nanoparticles, PMA- TiO_2 (20.0 mg TiO_2), and SAA- TiO_2 (5.0 mg TiO_2). The use of UV-Vis absorbance curves for evaluating the concentration of organic dyes in solution under irradiation are illustrated as follows for 20.0 mg of freely dispersed TiO_2 nanoparticles as the photocatalyst.

The UV-Vis absorbance curves of MO subjected to treatment at different irradiation times using 20.0 mg of freely dispersed TiO_2 nanoparticles as the photocatalyst are presented in Figure 7a. We note that MO strongly absorbs light in the range of 350–550 nm, and the maximum optical absorption peak is around 465 nm. Here, the spectrum labeled “–30 min” in Figure 7a was obtained after holding the suspension in the dark for 30 min prior to applying irradiation to ensure a physical adsorption-desorption balance between the TiO_2 nanoparticles and the MO in solution. In contrast, the spectrum labeled “0 min” was obtained immediately after adding the TiO_2 nanoparticles into the MO solution, and all subsequent spectra were obtained over time. It can be seen that the optical absorbance of MO is nearly unchanged after 30 min in the dark, which demonstrates that MO undergoes only weak physical adsorption on the TiO_2 nanoparticle surfaces. However, the optical absorbance of the solution decreased significantly under irradiation and was nearly zero after 60 min of irradiation. According to the Beer–Lambert law, the concentration of a compound in solution is proportional to the optical absorbance characteristic of that compound. Therefore, the results in Figure 7a indicate that most of the MO dye had been degraded. This is further illustrated in Figure 7b, which presents images of the MO

solution before and after irradiation treatment for 60 min. We note that the color of the MO solution faded significantly after 60 min of irradiation, indicating that the MO in the solution was degraded.

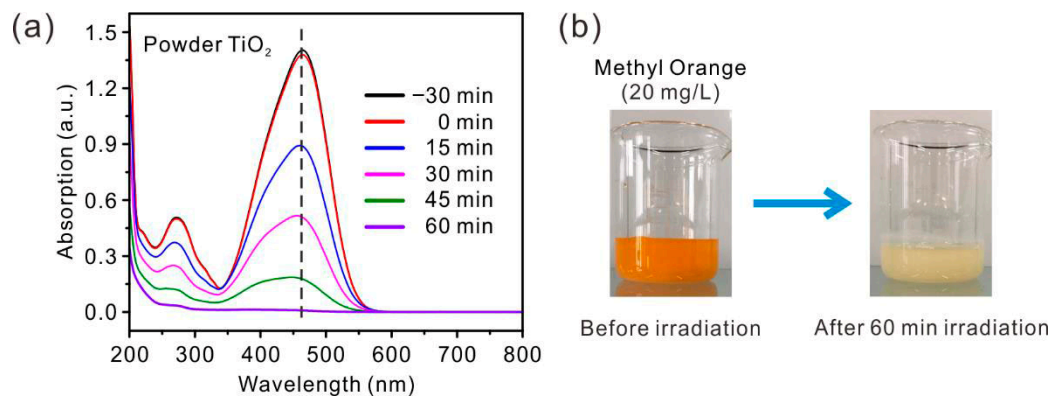


Figure 7. (a) UV-Vis absorbance curves of methyl orange (20 mg/L) subjected to treatment at different irradiation times using 20.0 mg of freely dispersed TiO₂ nanoparticles as the photocatalyst. Here, the spectrum labeled “−30 min” was obtained after holding the suspension in the dark for 30 min prior to applying irradiation to ensure an adsorption-desorption balance, while the spectrum labeled “0 min” was obtained immediately after adding the nanoparticles into the methyl orange solution. (b) Color change of the methyl orange solution before and after irradiation treatment for 60 min.

Because the maximum optical absorption peak of MO is around 465 nm, changes in the optical absorbance of the solution at 465 nm was employed to evaluate the concentration of MO in solution with respect to time under irradiation for the photocatalysts considered. Similarly, the maximum optical absorption peak of methylene blue is at 664 nm, and the optical absorbance of methylene blue solutions at this wavelength was employed to evaluate the concentration of methylene blue in solution with respect to time under irradiation for the photocatalysts considered. Finally, we evaluated the optical absorbance of RhB solutions at 554 nm and that of bright green solutions at 624 nm.

The dye concentration results obtained using freely dispersed TiO₂ nanoparticles (20.0 mg) and PMA-TiO₂ (20.0 mg) as the photocatalysts for MO, methylene blue, RhB, and bright green dye solutions are presented in Figure S1a–d, respectively. We note from Figure S1a that the photocatalytic efficiency of PMA-TiO₂ for MO was about 40.3% that of the freely dispersed TiO₂ nanoparticles after 60 min. The results in Figure S1b demonstrate that the methylene blue dye was completely degraded after 45 min of irradiation when freely dispersed TiO₂ nanoparticles were used as the photocatalyst, while the photocatalytic efficiency of PMA-TiO₂ was 61.4% that of the TiO₂ nanoparticles after 60 min. The results in Figure S1c demonstrate that the photodegradation rates obtained for RhB after 60 min of irradiation were 97.8% and 88.2% for the freely dispersed TiO₂ nanoparticles and PMA-TiO₂, respectively. As such, while the photocatalytic efficiency of PMA-TiO₂ was less than that of the TiO₂ nanoparticles for the RhB dye, it was nonetheless very similar. As discussed above, the decreased photocatalytic efficiency of PMA-TiO₂ for the MO, methylene blue, and RhB dyes can be attributed to the reduced availability of light owing to the immobilization of the TiO₂ nanoparticles. Finally, the results in Figure S1d represent highly contrasting results, where the photodegradation rates obtained for bright green after 60 min of irradiation were 33.9% and 73.9% for the freely dispersed TiO₂ nanoparticles and PMA-TiO₂, respectively. However, we also note that the concentration of bright green had already decreased by 73.9% prior to irradiation when employing PMA-TiO₂ as the photocatalyst because of the very high physical adsorption capacity of PMA-TiO₂ for bright green dye. Unfortunately, this also means that the actual level of degradation cannot be known with certainty because the decreased concentration in the solution can be due to physical adsorption, photodegradation, or both. However, we note that the physical

absorption observed for the other three organic dyes on PMA-TiO₂ prior to irradiation was considerably less than that observed for bright green, while the concentrations of all three decreased rapidly during irradiation due to the continuous uptake of solution. Therefore, these results suggest that the decrease in the bright green concentration during illumination was primarily due to photocatalytic reactions with the PMA-TiO₂ catalyst. These results also suggest that the very high physical adsorption capacity of PMA-TiO₂ for bright green dye counteracted the diminished photocatalytic efficiency of PMA-TiO₂ for the dye due to the reduced availability of light caused by the immobilization of the TiO₂ nanoparticles.

The dye concentration results obtained using freely dispersed TiO₂ nanoparticles (5.0 mg) and SAA-TiO₂ (5.0 mg) as the photocatalysts for MO, methylene blue, RhB, and bright green dye solutions are presented in Figure S2a–d, respectively. As expected, the overall photocatalytic efficiency of both catalysts is considerably less than that observed in Figure S1, owing to greatly reduced TiO₂ nanoparticle content. However, the general trends observed in Figure S2 for the photodegradation of all four organic dyes are quite similar to those observed in Figure S1. In the case of MO, methylene blue, and RhB, the degradation rates obtained after continuous irradiation for 60 min by the freely dispersed TiO₂ nanoparticles were 52.6%, 73.1%, and 68.8%, respectively, while the corresponding degradation rates obtained by SAA-TiO₂ were 26.6%, 51.5%, and 50.7%, respectively. Accordingly, the degradation rates obtained by the freely dispersed TiO₂ nanoparticles were greater than those obtained by SAA-TiO₂ for all three of these organic dyes. However, the photocatalytic efficiency of SAA-TiO₂ was close to that of the freely dispersed TiO₂ nanoparticles for RhB, as was observed in Figure S1c for PMA-TiO₂. In contrast, the degradation rate obtained after continuous irradiation for 60 min by the freely dispersed TiO₂ nanoparticles for bright green was only 13.2%, while that obtained by SAA-TiO₂ was nearly 90%. However, as was observed in Figure S1d, the concentration of bright green had already decreased by 35.0% prior to irradiation due to its physical adsorption by the SAA hydrogel. Accordingly, the actual photodegradation efficiency of SAA-TiO₂ for bright green dye is difficult to determine.

The above results demonstrate that the PMA-TiO₂ and SAA-TiO₂ samples have slightly greater physical adsorption capacities for MO, methylene blue, and RhB than the freely dispersed TiO₂ nanoparticles, while the adsorption capacities were considerably greater for bright green. Moreover, the concentrations of the organic dyes gradually decrease under irradiation, indicating that the dye molecules continue to be absorbed by the PMA and SAA hydrogels, and interact with the embedded TiO₂ nanoparticles. Again, compared with powdered TiO₂, TiO₂ is fixed in the hydrogel, which reduces the effective light-receiving area. On the other hand, there was no magnetic stirring when the TiO₂-hydrogel sample was used for photocatalysis experiment. At the same time, in the process of photodegradation, the concentration of the solution near the hydrogel will gradually decrease, but the molecules in the distance will not be enough to diffuse, resulting in a certain concentration difference. The above two main factors will restrict the overall degradation efficiency, making the TiO₂-hydrogel catalyst less efficient than powdered TiO₂.

However, we must also note that magnetic stirring must be applied to maintain the full dispersal of TiO₂ nanoparticles in the solutions, while the hydrogel-TiO₂ samples were applied without magnetic stirring. This can be expected to induce the formation of unfavorable organic dye concentration gradients in the solution near the hydrogel-TiO₂ samples during the reaction process. Nonetheless, the photodegradation efficiencies of both PMA-TiO₂ and SAA-TiO₂ for RhB were very close to those of the freely dispersed TiO₂ nanoparticles when in equal concentrations. In the case of real industrial wastewater, different pH and temperatures of spent water may occur. Therefore, we evaluated the photodegradation properties of TiO₂-hydrogel under different temperatures and different pH. As shown in Figure S3a, the physical adsorption capacity of the hydrogel for methyl orange increases with the increase in temperature. At the same time, the degradation efficiency of the catalyst was enhanced by increasing the temperature. The degradation efficiencies of PMA-TiO₂ at ambient temperature of 10 °C, 25 °C, and 45 °C were 15.2%,

40.3%, and 63.1%, respectively. As shown in Figure S3b, the degradation performance of the catalyst is different under different pH conditions. The degradation efficiencies of PMA-TiO₂ were 28.1%, 40.3%, and 52.3%, respectively when the pH values were 4.0, 6.9, and 9.1, respectively.

The degradation-regeneration cycling performances of the PMA-TiO₂ (20.0 mg) and SAA-TiO₂ (5.0 mg) samples were evaluated, and the results of four cycles for the photodegradation of RhB are presented in Figure 8a,b, respectively. While not shown here, we note that the physical adsorption capacities of the two hydrogel-TiO₂ samples for RhB dye during the 30 min period of darkness prior to irradiation were nearly constant at the beginning of each cycle. The results in Figure 8 indicate that the RhB degradation rates obtained by PMA-TiO₂ after 1 h of irradiation were 88.2%, 84.4%, 77.2%, and 70.2% at each of the four cycles, respectively, while the corresponding values obtained by SAA-TiO₂ were 50.7%, 47.3%, 43.1%, and 35.7%, respectively. While the photocatalytic efficiency of the samples decreased slightly over the four cycles, the relative efficiencies of the PMA-TiO₂ and SAA-TiO₂ samples after the fourth cycle were 76.9% and 70.4%, respectively, of the efficiencies obtained in the first cycle. Accordingly, the proposed hydrogel-TiO₂ photocatalysts offer easy reuse without solid-liquid separation and provide satisfactory photodegradation efficiencies for RhB after as many as four cycles of use.

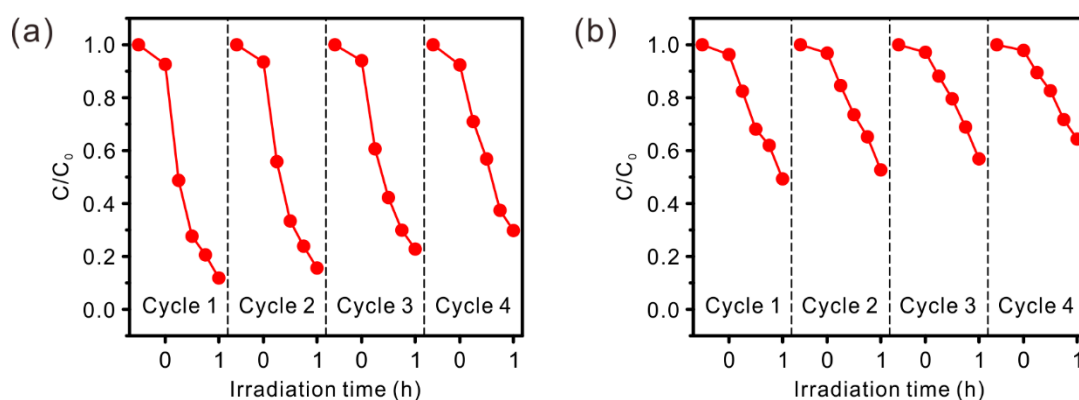


Figure 8. Cycling performance for the photodegradation of rhodamine B using (a) PMA-TiO₂ (20.0 mg) and (b) SAA-TiO₂ (5.0 mg).

3. Materials and Methods

3.1. Chemicals and Materials

Polyethylene glycol adipate (PEGA, AR), ethylene glycol monomethyl ether acrylate (MEA, 99.7%), acrylic acid (AA, ≥98%), acrylamide (AAM, ≥98%), ammonium persulfate (APS, ≥98%), and sodium salt (SA, CP) were purchased from Sinopharm Chemical Reagent Co., Ltd (Shanghai, China). Titanium dioxide (TiO₂, Degussa P25, 99.5%) and triethanolamine (TEOA, 99%) were purchased from Sigma-Aldrich (Shanghai, China). Methyl orange, methylene blue, rhodamine B, and bright green were purchased from Macklin (Shang, China). All chemicals were used without further purification.

3.2. Preparation of PMA Hydrogel and PMA-TiO₂

PMA hydrogel and PMA-TiO₂ were synthesized according to our previous work [30]. Precisely, 1.6 g polyethylene glycol adipate (PEGA) and 0.6 g ethylene glycol monomethyl ether acrylate (MEA) were dissolved in 5 mL of water at room temperature. After magnetic stirring for 10 min, 0.6 g of acrylic acid (AA) was slowly added. After stirring for 1 h, 3.0 g of the mixed solution was taken and 1.0 mL of ammonium persulfate aqueous solution (APS, 0.4 mol/L) was slowly added. The solution was transferred to an oven (50 °C) after magnetic stirring for 0.5 h. The PMA hydrogel would be obtained within several hours. To make the surface clean, the PMA hydrogel was washed with deionized water and then

dried at 60 °C for 12 h. The PMA-TiO₂ sample was obtained with the same method except for the addition of 10.0 mg or 20.0 mg of TiO₂ powder before adding the APS solution.

3.3. Preparation of SAA Hydrogel and SAA-TiO₂ Hydrogel

SAA hydrogel and SAA-TiO₂ were synthesized according to our previous work [30]. Precisely, 4.5 g of sodium alginate were dissolved in a beaker at room temperature. Under magnetic stirring, 2.0 g of acrylamide (AAM), 4.0 g of acrylic acid (AA), and 1.0 mL of deionized water were slowly added. After stirring for 1 h, 3.0 g of the mixed solution was taken and 1.0 mL of ammonium persulfate aqueous solution (APS, 0.4 mol/L) was slowly added. The solution was transferred to an oven (50 °C) after magnetic stirring for 0.5 h. The SAA hydrogel was obtained within several hours. To make the surface clean, the SAA hydrogel was washed with deionized water and then dried at 60 °C for 12 h. The SAA-TiO₂ sample was obtained with the same method, except with the addition of 5.00 mg of TiO₂ powder before adding the APS solution.

4. Conclusions

The present study addressed the underreported use of hydrogels in wastewater treatment applications based on photocatalytic degradation by developing PMA and SAA hydrogels with embedded TiO₂ nanoparticles. The photodegradation efficiencies obtained by the hydrogel-TiO₂ samples were less than those obtained by equivalent concentrations of freely dispersed TiO₂ nanoparticles in solution for the four organic dyes considered. Nevertheless, the photodegradation efficiencies of both PMA-TiO₂ and SAA-TiO₂ for RhB were very close to those of the freely dispersed TiO₂ nanoparticles. While the photocatalytic efficiencies of the PMA-TiO₂ and SAA-TiO₂ samples for RhB decreased slightly over the four degradation-regeneration cycles, their relative efficiencies after the fourth cycle were 76.9% and 70.4%, respectively, of the efficiencies obtained in the first cycle. Accordingly, the excellent solution absorption of the proposed hydrogel-TiO₂ photocatalysts facilitates the uptake of solutions, which enables photocatalytic reactions with the uniformly embedded TiO₂ nanoparticles. As a result, the photocatalysts can be easily reused without solid-liquid separation and provide satisfactory photodegradation efficiencies for RhB after as many as four cycles of use.

Supplementary Materials: The following are available online at <https://www.mdpi.com/article/10.3390/catal11050613/s1>, Figure S1: Photodegradation efficiency of (a) methyl orange, (b) methylene blue, (c) rhodamine B, and (d) bright green by powdery TiO₂ and PMA-TiO₂ (20.0 mg) hydrogel, respectively. C₀ represents the initial concentration of the organic dyes and C represents the real-time concentration. Figure S2: Photodegradation efficiency of (a) methyl orange, (b) methylene blue, (c) rhodamine B, and (d) bright green by powdery TiO₂ and SAA-TiO₂ (5.0 mg) hydrogel, respectively. C₀ represents the initial concentration of the organic dyes and C represents the real-time concentration. **Figure S3:** Catalytic performance of PMA-TiO₂ at (a) different temperatures and (b) different pH.

Author Contributions: X.Y. & H.H. contributed equally. Methodology, software, validation, formal analysis, data curation, X.Y. and H.H.; Investigation, X.Y., H.H., R.Z. and Z.Y.; writing—original draft preparation, X.Y.; conceptualization, resources, writing—review and editing, visualization, supervision, project administration, funding acquisition, M.X., X.W. and Y.Y. All authors have read and agreed to the published version of the manuscript.

Funding: This work was financially supported by the National Natural Science Foundation of China (Grant No. 22072045 and 21574043), the Ministry of Science and Technology of the People's Republic of China (Grant No. 2018YFF01012504), and the Fundamental Research Funds for the Central Universities.

Data Availability Statement: The data presented in this study are available on request from the corresponding author. The data are not publicly available due to restrictions of the institution's privacy policy.

Acknowledgments: The authors would like to thank the laboratories that supported this work: Physics Department & Shanghai Key Laboratory of Magnetic Resonance.

Conflicts of Interest: The authors declare no conflict of interest.

References

1. Schwarzenbach, R.P.; Egli, T.; Hofstetter, T.B.; von Gunten, U.; Wehrli, B. Global Water Pollution and Human Health. *Annu. Rev. Environ. Resour.* **2010**, *35*, 109–136. [[CrossRef](#)]
2. Allman, A.; Daoutidis, P.; Arnold, W.A.; Cussler, E.L. Efficient Water Pollution Abatement. *Ind. Eng. Chem. Res.* **2019**, *58*, 22483–22487. [[CrossRef](#)]
3. Panahi, Y.; Mellatyar, H.; Farshbaf, M.; Sabet, Z.; Fattahi, T.; Akbarzadehe, A. Biotechnological applications of nanomaterials for air pollution and water/wastewater treatment. *Mater. Today Proc.* **2018**, *5*, 15550–15558. [[CrossRef](#)]
4. Konstantinou, I.K.; Albanis, T.A. TiO₂-assisted photocatalytic degradation of azo dyes in aqueous solution: Kinetic and mechanistic investigations—A review. *Appl. Catal. B Environ.* **2004**, *49*, 1–14. [[CrossRef](#)]
5. Pan, T.D.; Li, Z.J.; Shou, D.H.; Shou, W.; Fan, J.T.; Liu, X.; Liu, Y. Buoyancy Assisted Janus Membrane Preparation by ZnO Interfacial Deposition for Water Pollution Treatment and Self-cleaning. *Adv. Mater. Interfaces* **2019**, *6*, 1901130. [[CrossRef](#)]
6. Kudlek, E.; Dudziak, M. Degradation pathways of pentachlorophenol and benzo(a)pyrene during heterogeneous photocatalysis. *Water Sci. Technol.* **2018**, *77*, 2407–2414. [[CrossRef](#)]
7. Wang, J.C.; Cui, C.X.; Kong, Q.Q.; Ren, C.Y.; Li, Z.J.; Qu, L.B.; Zhang, Y.P.; Jiang, K. Mn-Doped g-C₃N₄ Nanoribbon for Efficient Visible-Light Photocatalytic Water Splitting Coupling with Methylene Blue Degradation. *ACS Sustain. Chem. Eng.* **2018**, *6*, 8754–8761. [[CrossRef](#)]
8. Ni, M.; Leung, M.K.H.; Leung, D.Y.C.; Sumathy, K. A review and recent developments in photocatalytic water-splitting using TiO₂ for hydrogen production. *Renew. Sustain. Energy Rev.* **2007**, *11*, 401–425. [[CrossRef](#)]
9. Boccuzzi, F.; Chiorino, A.; Manzoli, M.; Andreeva, D.; Tabakova, T.; Ilieva, L.; Iadakov, V. Gold, silver and copper catalysts supported on TiO₂ for pure hydrogen production. *Catal. Today* **2002**, *75*, 169–175. [[CrossRef](#)]
10. Zhang, Z.Y.; Zuo, F.; Feng, P.Y. Hard template synthesis of crystalline mesoporous anatase TiO₂ for photocatalytic hydrogen evolution. *J. Mater. Chem.* **2010**, *20*, 2206–2212. [[CrossRef](#)]
11. Ge, M.Z.; Li, Q.S.; Cao, C.Y.; Huang, J.Y.; Li, S.H.; Zhang, S.N.; Chen, Z.; Zhang, K.Q.; Al-Deyab, S.S.; Lai, Y.K. One-dimensional TiO₂ Nanotube Photocatalysts for Solar Water Splitting. *Adv. Sci.* **2017**, *4*, 1600152. [[CrossRef](#)]
12. Yoong, L.S.; Chong, F.K.; Dutta, B.K. Development of copper-doped TiO₂ photocatalyst for hydrogen production under visible light. *Energy* **2009**, *34*, 1652–1661. [[CrossRef](#)]
13. Cho, I.S.; Chen, Z.B.; Forman, A.J.; Kim, D.R.; Rao, P.M.; Jaramillo, T.F.; Zheng, X.L. Branched TiO₂ Nanorods for Photoelectrochemical Hydrogen Production. *Nano Lett.* **2011**, *11*, 4978–4984. [[CrossRef](#)]
14. Haider, A.J.; Al-Anbari, R.H.; Kadhim, G.R.; Salame, C.T. Exploring potential Environmental applications of TiO₂ Nanoparticles. *Energy Procedia* **2017**, *119*, 332–345. [[CrossRef](#)]
15. Lucic, M.; Milosavljevic, N.; Radetic, M.; Saponjic, Z.; Radoicic, M.; Krusic, M.K. The potential application of TiO₂/hydrogel nanocomposite for removal of various textile azo dyes. *Sep. Purif. Technol.* **2014**, *122*, 206–216. [[CrossRef](#)]
16. Byrne, J.A.; Eggins, B.R.; Brown, N.M.D.; McKinney, B.; Rouse, M. Immobilisation of TiO₂ powder for the treatment of polluted water. *Appl. Catal. B Environ.* **1998**, *17*, 25–36. [[CrossRef](#)]
17. Li, D.W.; Zheng, H.Y.; Wang, Q.H.; Wang, X.; Jiang, W.Z.; Zhang, Z.Y.; Yang, Y.N. A novel double-cylindrical-shell photoreactor immobilized with monolayer TiO₂-coated silica gel beads for photocatalytic degradation of Rhodamine B and Methyl Orange in aqueous solution. *Sep. Purif. Technol.* **2014**, *123*, 130–138. [[CrossRef](#)]
18. Lei, P.; Wang, F.; Gao, X.W.; Ding, Y.F.; Zhang, S.M.; Zhao, J.C.; Liu, S.R.; Yang, M.S. Immobilization of TiO₂ nanoparticles in polymeric substrates by chemical bonding for multi-cycle photodegradation of organic pollutants. *J. Hazard. Mater.* **2012**, *227*, 185–194. [[CrossRef](#)] [[PubMed](#)]
19. Gupta, V.K.; Gupta, B.; Rastogi, A.; Agarwal, S.; Nayak, A. A comparative investigation on adsorption performances of mesoporous activated carbon prepared from waste rubber tire and activated carbon for a hazardous azo dye-Acid Blue 113. *J. Hazard. Mater.* **2011**, *186*, 891–901. [[CrossRef](#)] [[PubMed](#)]
20. Yun, J.; Im, J.S.; Oh, A.; Jin, D.H.; Bae, T.S.; Lee, Y.S.; Kim, H.I. pH-sensitive photocatalytic activities of TiO₂/poly(vinyl alcohol)/poly(acrylic acid) composite hydrogels. *Mater. Sci. Eng. B Adv.* **2011**, *176*, 276–281. [[CrossRef](#)]
21. Weingarten, A.S.; Kazantsev, R.V.; Palmer, L.C.; McClendon, M.; Koltonow, A.R.; Samuel, A.P.S.; Kiebal, D.J.; Wasielewski, M.R.; Stupp, S.I. Self-assembling hydrogel scaffolds for photocatalytic hydrogen production. *Nat. Chem.* **2014**, *6*, 964–970. [[CrossRef](#)]
22. Yun, J.; Jin, D.; Lee, Y.S.; Kim, H.I. Photocatalytic treatment of acidic waste water by electrospun composite nanofibers of pH-sensitive hydrogel and TiO₂. *Mater. Lett.* **2010**, *64*, 2431–2434. [[CrossRef](#)]
23. Jiang, W.J.; Liu, Y.F.; Wang, J.; Zhang, M.; Luo, W.J.; Zhu, Y.F. Separation-Free Polyaniline/TiO₂ 3D Hydrogel with High Photocatalytic Activity. *Adv. Mater. Interfaces* **2016**, *3*, 1500502. [[CrossRef](#)]
24. Omidian, H.; Rocca, J.G.; Park, K. Advances in superporous hydrogels. *J. Control. Release* **2005**, *102*, 3–12. [[CrossRef](#)] [[PubMed](#)]
25. Zeng, X.K.; McCarthy, D.T.; Deletic, A.; Zhang, X.W. Silver/Reduced Graphene Oxide Hydrogel as Novel Bactericidal Filter for Point-of-Use Water Disinfection. *Adv. Funct. Mater.* **2015**, *25*, 4344–4351. [[CrossRef](#)]

26. Chen, Q.; Zhu, L.; Zhao, C.; Wang, Q.M.; Zheng, J. A Robust, One-Pot Synthesis of Highly Mechanical and Recoverable Double Network Hydrogels Using Thermoreversible Sol-Gel Polysaccharide. *Adv. Mater.* **2013**, *25*, 4171–4176. [[CrossRef](#)]
27. Worsley, M.A.; Shin, S.J.; Merrill, M.D.; Lenhardt, J.; Nelson, A.J.; Woo, L.Y.; Gash, A.E.; Baumann, T.F.; Orme, C.A. Ultra low Density, Monolithic WS₂, MoS₂, and MoS₂/Graphene Aerogels. *ACS Nano* **2015**, *9*, 4698–4705. [[CrossRef](#)]
28. Liu, X.S.; Thomas, J.K. Synthesis of microporous titanosilicates ETS-10 and ETS-4 using solid TiO₂ as the source of titanium. *Chem. Commun.* **1996**, *12*, 1435–1436. [[CrossRef](#)]
29. Van der Meulen, T.; Mattson, A.; Osterlund, L. A comparative study of the photocatalytic oxidation of propane on anatase, rutile, and mixed-phase anatase-rutile TiO₂ nanoparticles: Role of surface intermediates. *J. Catal.* **2007**, *251*, 131–144. [[CrossRef](#)]
30. Huang, H.L.; Hou, L.F.; Zhu, F.; Li, J.; Xu, M. Controllable thermal and pH responsive behavior of PEG based hydrogels and applications for dye adsorption and release. *RSC Adv.* **2018**, *8*, 9334–9343. [[CrossRef](#)]